JACS
JOURNAL OF THE AMERICAN CHEMICAL SOCIETY
Communication
pubs.acs.org/JACS

# In Situ Growth of Metal Particles on 3D Urchin-like $WO_3$ Nanostructures

Guangcheng Xi,[†,‡] Jinhua Ye,*[,†,§] Qiang Ma,[‡] Ning Su,[‡] Hua Bai,[‡] and Chao Wang[‡]

[†]International Center for Materials Nanoarchitectonics and Photocatalytic Materials Center, National Institute for Materials Science, 1-2-1 Sengen, Tsukuba, Ibaraki 305-0047, Japan

[‡]Nanomaterials and Nanoproducts Inspection and Research Center, Chinese Academy of Inspection and Quarantine (CAIQ), Beijing 100123, P.R. China

[§]TU-NIMS Joint Research Center, School of Materials Science and Engineering, Tianjin University, 92 Weijin Road, Nankai District, Tianjin, P.R. China

Supporting Information

**ABSTRACT:** Metal/semiconductor hybrid materials of various sizes and morphologies have many applications in areas such as catalysis and sensing. Various organic agents are necessary to stabilize metal nanoparticles during synthesis, which leads to a layer of organic compounds present at the interfaces between the metal particles and the semiconductor supports. Generally, high-temperature oxidative treatment is used to remove the organics, which can extensively change the size and morphology of the particles, in turn altering their activity. Here we report a facile method for direct growth of noble-metal particles on $WO_3$ through an in situ redox reaction between weakly reductive $WO_{2.72}$ and oxidative metal salts in aqueous solution. This synthetic strategy has the advantages that it takes place in one step and requires no foreign reducing agents, stabilizing agents, or pretreatment of the precursors, making it a practical method for the controlled synthesis of metal/semiconductor hybrid nanomaterials. This synthetic method may open up a new way to develop metal-nanoparticle-loaded semiconductor composites.

Metal/semiconductor hybrid nanoparticles with various morphologies and sizes have many applications, including CO oxidation,[1,2] water splitting,[3,4] and environmental protection.[5−7] Organic agents, such as polymers and surfactants, are necessary to stabilize metal nanoparticles during synthesis, which leads to the presence of an organic layer at the interfaces between the metal particles and the supports. The bad contact leads to uncertainties in regard to improving the efficiency of charge separation and transport. To date, removal of these stabilizing molecules has been successfully achieved only by using thermal and oxidative methods.[8] Such methods lead to significant changes in the size and morphology of the hybrid particles that often extensively negate their catalytic efficacy.[2] Alternatively, if a metal particle could be directly grown over a semiconductor substrate through an in situ redox reaction without any foreign reducing agents or stabilizing molecules, the catalytic activity of the resulting hybrid composite would be significantly enhanced.

Our inspiration raise from the following idea: for most types of transition metal oxides, their low valence state or nonstoichiometric members often have strong or weak reducing power. Therefore, we could first synthesize a low-valence-state or nonstoichiometric species of an oxide with a desirable morphology. The reductive oxide could then react with the oxidative noble-metal salt in aqueous solution. By this in situ redox reaction, it should be possible to grow noble-metal particles directly on the oxide surface.

Here we report a facile method for the direct growth of metal particles on $WO_3$ through an in situ redox reaction between weakly reductive $WO_{2.72}$ and oxidative metal salt precursors in aqueous solution. No foreign reducing agents or stabilizing agents are required, avoiding the introduction of impurities and ensuring that the metal−$WO_3$ interfaces are clean.

The general pathway used to fabricate metal/$WO_3$ composites is shown in Scheme 1. The noble-metal-loaded

**Scheme 1. Schematic Procedure for in Situ Loading of Metal Particles on $WO_3$**

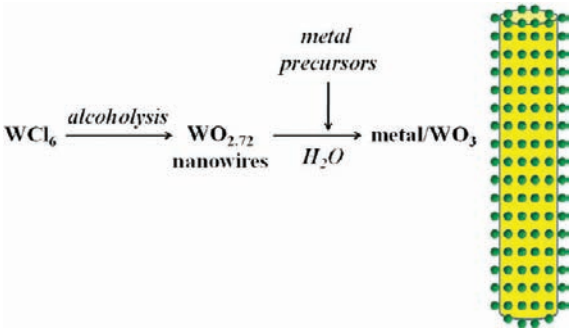


$WO_3$ composites were prepared in two steps: (1) $WCl_6$ alcoholysis was first used to synthesize the $WO_{2.72}$ nanostructure, which has a weak reducing ability; (2) the as-synthesized $WO_{2.72}$ nanostructures and metal salts were then mixed in aqueous solution at room temperature. Once the metal ions came into contact with the $WO_{2.72}$ nanostructures, they were immediately reduced and nucleated rapidly on its surface, growing into clusters and further into nanoparticles. Mean-

Received: December 13, 2011
Published: April 3, 2012

   dx.doi.org/10.1021/ja211638e | J. Am. Chem. Soc. 2012, 134, 6508−6511

while, the support was partially oxidized by the metal ions and further converted completely into $WO_3$ after exposure to air, resulting metal/$WO_3$ nanocomposites.

$WO_{2.72}$ is a monoclinic-type structure ($P2/m$) with lattice parameters of $a$ = 18.318 Å, $b$ = 3.782 Å, and $c$ = 14.028 Å.[9] The monoclinic $WO_{2.72}$ consists of an ordered 2D lattice of edge-sharing distorted $WO_6$ octahedra that form a network of pentagonal columns interspersed with hexagonal channels [Figure S1a in the Supporting Information (SI)]. The X-ray diffraction (XRD) pattern of our sample displays mainly two intense diffraction peaks, corresponding to the (010) and (020) crystal faces of the monoclinic $WO_{2.72}$ structure (JCPDS no. 36-101) (Figure S1b).[10] All of the other diffraction peaks are much weaker, resulting in broad diffraction peaks. The narrow (010) and (020) diffraction peaks strongly suggest that the possible crystal growth direction of the sample is [010], since the close-packed planes of the monoclinic $WO_{2.72}$ crystal are {010},[11] as will be further demonstrated by the following high-resolution transmission electron microscopy (HRTEM) analysis.

The scanning electron microscopy (SEM) image shows that the as-synthesized $WO_{2.72}$ is an urchin-like hierarchical structure (Figure 1a and Figure S2). The TEM image further

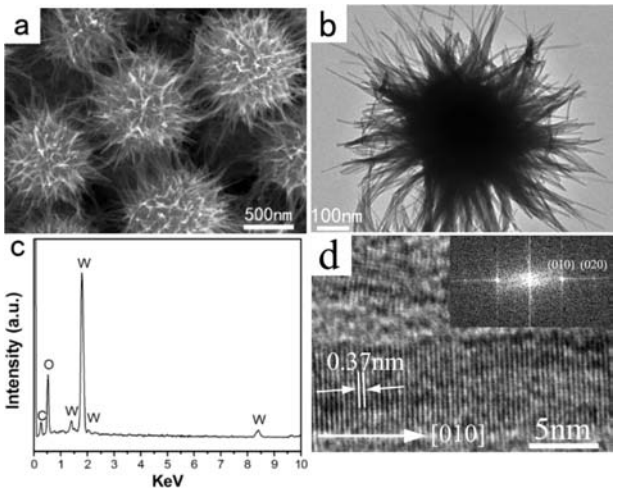


**Figure 1.** (a) SEM and (b) TEM images of the $WO_{2.72}$ sample. (c) EDS spectrum of the sample. (d) HRTEM image and (inset) corresponding FFT pattern of a $WO_{2.72}$ nanowire.

shows that the hierarchical structure is composed of a large number of radial nanowires (Figure 1b and Figure S3). The nanowires are 5−15 nm in diameter and ∼600 nm in length. Energy-dispersive X-ray spectroscopy (EDS) (Figure 1c) confirms that the sample contains only the elements W and O. The HRTEM image and corresponding FFT pattern (Figure 1d and Figure S4) further confirm the single-crystalline nature of the $WO_{2.72}$ nanowires. The spacing between adjacent lattice planes is 0.37 nm, corresponding to the (010) planes of monoclinic $WO_{2.72}$, which indicates that the preferential growth direction is [010].

The $WO_{2.72}$ nanowires were further characterized by nitrogen adsorption and desorption isotherms at 77 K (Figure S5). It was found that the urchin-like $WO_{2.72}$ has a high Brunauer−Emmett−Teller surface area of 102 $m^2\ g^{-1}$, which is a favorable factor for catalysis. In addition, the Fourier transform IR (FTIR) spectrum exhibits no organics coated on the surface of the $WO_{2.72}$ (Figure S6).

The UV−vis−NIR absorption spectrum of the as-synthesized $WO_{2.72}$ is shown in Figure S7. Very interestingly, the considerably large absorption tail present in the visible and NIR regions gives clear evidence that the nonstoichimetric $WO_{2.72}$ contains a large number of oxygen vacancies,[12] the presence of which suggests that the urchin-like $WO_{2.72}$ has reducing power.

The urchin-like $WO_{2.72}$ was reacted with metal precursors at room temperature. The obtained metal/$WO_3$ hybrid composites with a metal (M) content of $A$ wt % and mean particle size of $B$ nm is denoted as M/$WO_3$ ($A$ wt %, $B$ nm). Figure 2a

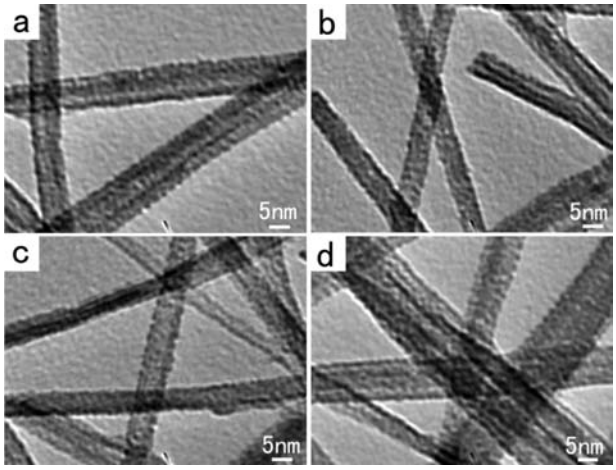


**Figure 2.** TEM images of metal/$WO_3$ composites: (a) Pt/$WO_3$ (0.9 wt %, <1 nm), (b) Au/$WO_3$ (1.1 wt %, <1 nm), (c) Rh/$WO_3$ (1.0 wt %, <1 nm), (d) Ag/$WO_3$ (0.8 wt %, <1 nm).

shows a typical TEM image of a Pt/$WO_3$ (0.9 wt %, <1 nm) composite, which clearly displays the homogeneous depostion of Pt particles throughout the $WO_3$ substrate. The Pt particles are so small that we only roughly describe their size as $B$ < 1 nm. The XRD pattern shows that the hybrid $WO_3$ nanowires are monoclinic (Figure S8). The Pt particles were not detected by XRD because their amount is less than the resolution of the instrument (∼1.5%) and their size is very small. We also prepared Au/$WO_3$, Rh/$WO_3$, and Ag/$WO_3$ hybrid composites using the method described above. TEM images of these samples (Figure 2b−d) show that the surfaces of $WO_3$ nanowires are decorated with numerous nanoparticles having an ultrathin size and a very narrow size distribution. The EDS spectra shown in Figure S9 confirm that the samples contain only W, O, and the corresponding metal elements. The as-synthesized hybrid composites can be easily isolated and redispersed in appropriate solvents such as water and ethanol for applications (Figure S10).

A two-step injection process was used to introduce the metal precursor in this method (for details of the experimental procedures for growing noble-metal particles on the surface of $WO_3$, see the SI). As a result of the rapid nucleation on $WO_{2.72}$, a large number of ultrathin nuclei were formed in situ on the substrate as the first portion of the precursor was injected, and these served as seeds for the growth of the metal particles as more precursor was introduced. The metal particle size can be readily tuned by changing the total amount of the precursor,. Experiments showed that when the amount of the first injection was kept unchanged, the size of the metal particles on the surface of the $WO_3$ nanowires generally increased as the


dx.doi.org/10.1021/ja211638e | J. Am. Chem. Soc. 2012, 134, 6508−6511

amount of the second injection increased. Thus, increasing the amount of the second injection allowed $Pt/WO_3$ hybrid composites with a larger Pt particle size distribution to be prepared in a controlled fashion (Figure 3a,b and Figure S11).

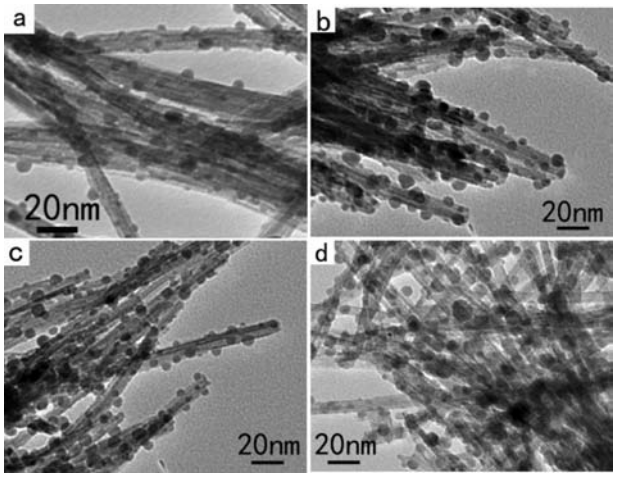


**Figure 3.** TEM images of $WO_3$ architectures loaded with larger-sized metal particles: (a) $Pt/WO_3$ (1.7 wt %, 3.5 nm); (b) $Pt/WO_3$ (2.1 wt %, 5 nm); (c) $Ag/WO_3$ (1.8 wt %, 3 nm); (d) $Au/WO_3$ (2.6 wt %, 5 nm).

Other noble-metal-particle-loaded $WO_3$ with different metal particle size distributions also can be synthesized by adjusting the amount of the second injection. For example, larger-sized Ag- and Au-particle-loaded $WO_3$ hybrid composites were fabricated by this method (Figure 3c,d). Comparison of Figures 2 and 3 shows that the metal nanoparticle density significantly decreases with increasing particle size. This phenomenon could be attributed to the well-known Ostwald ripening process, which is illustrated in Figure S12. Furthermore, controlled experiments showed that only disordered aggregates are obtained when all of the precursor is added in one step (Figure S13). In addition, HRTEM images (Figure S14–S15) show that the larger metal nanoparticles have higher crystallinity than that of the smaller metal nanoparticles, which may be attributed to their longer aging time.

The photocatalytic degradation of toxic pollutants is of great significance in environmental pollutant treatment and represents a commonly used approach to characterize the activity of photocatalysts. The photocatalytic activities of the as-synthesized metal/$WO_3$ samples were evaluated for degradation of rhodamine B (RhB) under visible-light irradiation ($\lambda \geq$ 420 nm), and the results were compared with RhB photolysis (without photocatalyst) and with those obtained over bare $WO_3$ nanowires and N-doped $TiO_2$ (Figure 4). Within 50 min of visible-light irradiation, the percentages of RhB degraded by bare $WO_3$ nanowires and N-doped $TiO_2$ were 30.2 and 40.3%, respectively. Significantly larger percentages of RhB were degraded with the $Rh/WO_3$, $Au/WO_3$, $Pt/WO_3$, and $Ag/WO_3$ samples. For the degradation of methyl orange (MO), methylene blue (MB), and acid fuchsin (AF), the metal/$WO_3$ hybrid materials also showed significantly enhanced photocatalytic activities. In addition, it was observed that the photolysis of RhB under visible-light irradition was very slow and that RhB cannot be degraded under dark conditions in the presence of the photocatalysts, confirming that the photocatalytic activity indeed originates from the metal/$WO_3$ hybrid

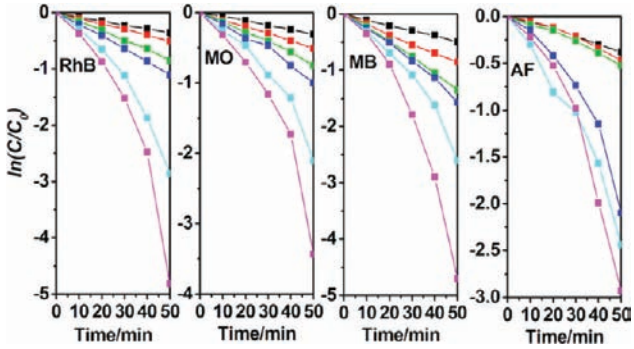


**Figure 4.** Photocatalytic activities of six catalysts for the RhB, MO, MB, and AF degradation reactions: bare $WO_3$ (black), N-doped $TiO_2$ (red), $Rh/WO_3$ (1.5 wt %, 3.8 nm) (green), $Pt/WO_3$ (1.7 wt %, 3.5 nm) (blue), $Au/WO_3$ (2.6 wt %, 5 nm) (cyan), $Ag/WO_3$ (1.8 wt %, 3 nm) (magenta).

materials. The enhanced photocatalytic activity of the $Au/WO_3$ and $Ag/WO_3$ hybrid materials probably results from the surface plasmon resonance (SPR) effect of metal nanoparticles. However, the enhanced visible-light photocatalytic properties of $Pt/WO_3$ and $Rh/WO_3$ might not result from their SPR effects because the SPR bands of Pt and Rh are in the UV region. Recent studies found that Pt-nanoparticle-modified $WO_3$ greatly enhanced the visible-light photocatalytic activity, which is attributed to a multielectron transfer mechanism induced by the loaded Pt or Cu nanoparticles.[13,14] Therefore, the enhanced photocatalytic activities of $Pt/WO_3$ and $Rh/WO_3$ probably result from the multielectron transfer mechanism. At the same time, the high electron conductivity of the metal particles also helps to improve the photogenerated electron/hole separation process. The catalytic efficiency of the hybrid materials does not significantly decrease even after they have been used to catalyze 10 reactions.

In conclusion, we have developed a facile method for direct growth of metal particles on metal oxides in situ. Through an in situ redox reaction between the weakly reductive $WO_{2.72}$ support and metal salt precursors, a series of noble metal/$WO_3$ nanocomposites with uniform metal dispersion, tunable metal particle size, and narrow metal particle size distribution were obtained. We believe this method can be used as a new way to prepare high-quality metal-particle-loaded semiconductor composites. The as-synthesized metal/$WO_3$ hybrid composites have superior visible-light photocatalytic performance. Further application of the metal/$WO_3$ nanocomposites to other catalysis, such as partial oxidation and cracking of hydrocarbons, catalytic combustion, and surface enhanced Raman spectroscopy (SERS) seems possible.

## ■ ASSOCIATED CONTENT

### Ⓢ Supporting Information

Experimental procedures and Figures S1–S15. This material is available free of charge via the Internet at http://pubs.acs.org.

## ■ AUTHOR INFORMATION

### Corresponding Author

Jinhua.Ye@nims.go.jp

### Notes

The authors declare no competing financial interest.

## ■ ACKNOWLEDGMENTS

This work received financial support from the World Premier International Research Center (WPI) Initiative on Materials Nanoarchitectonics, the Natural Science Foundation of China (51102220), the Dean Fund of CAIQ (2012JK023), the Science Foundation of AQSIQ (2012IK056), the Research Fund for Public Welfare Projects (201010021), and the Global COE Program of Tokyo Institute of Technology, Japan.

## ■ REFERENCES

(1) Herzing, A. A.; Kiely, C. J.; Carley, A. F.; Landon, P.; Hutchings, G. J. *Science* **2008**, *321*, 1331−1335.
(2) Lopez-Sanchez, J. A.; Dimitratos, N.; Hammond, C.; Brett, G. L.; Kesavan, L.; White, S.; Miedziak, P.; Tiruvalam, R.; Jenkins, R. L.; Carley, A. F.; Knight, D.; Kiely, C. J.; Hutchings, G. J. *Nat. Chem.* **2011**, *3*, 551−556.
(3) Ingram, G. B.; Linic, S. *J. Am. Chem. Soc.* **2011**, *133*, 5202−5205.
(4) Zou, Z. G.; Ye, J. H.; Sayama, K.; Arakawa, H. *Nature* **2001**, *414*, 625−628.
(5) Wang, P.; Huang, B. B.; Qin, X. Y.; Zhang, X. Y.; Dai, Y.; Wei, J. Y.; Whangbo, M. H. *Angew. Chem., Int. Ed.* **2008**, *47*, 7931−7934.
(6) An, C. H.; Peng, S.; Sun, Y. G. *Adv. Mater.* **2010**, *22*, 2570−2574.
(7) Qu, Y. Q.; Chen, R.; Su, Q.; Duan, X. F. *J. Am. Chem. Soc.* **2011**, *133*, 16730−16733.
(8) Menard, L. D.; Xu, F.; Nuzzo, R. G.; Yang, J. C. *J. Catal.* **2006**, *243*, 64−73.
(9) Polleux, J.; Pinna, N.; Antonietti, M.; Niederberger, M. *J. Am. Chem. Soc.* **2005**, *127*, 15595−15601.
(10) Yella, A.; Tahir, M. N.; Meuer, S.; Zentel, R.; Berger, R.; Panthöfer, M.; Tremel, W. *J. Am. Chem. Soc.* **2009**, *131*, 17566−17575.
(11) Lee, K.; Seo, W. S.; Park, J. T. *J. Am. Chem. Soc.* **2003**, *125*, 3408−3409.
(12) Nutz, T.; Haase, M. *J. Phys. Chem. B* **2000**, *104*, 8430−8437.
(13) Abe, R.; Takami, H.; Murakami, N.; Ohtani, B. *J. Am. Chem. Soc.* **2008**, *130*, 7780−7781.
(14) Irie, H.; Miura, S.; Kamiya, K.; Hashimoto, K. *Chem. Phys. Lett.* **2008**, *457*, 202−206.